

Charge-loop current order and Z_3 nematicity mediated by bond-order fluctuations in kagome metal AV_3Sb_5 (A=Cs,Rb,K)

Rina Tazai, Youichi Yamakawa, and Hiroshi Kontani

Department of Physics, Nagoya University, Furo-cho, Nagoya 464-8602, Japan.

(Dated: December 5, 2023)

Recent experiments on geometrically frustrated kagome metal AV_3Sb_5 (A=K, Rb, Cs) have revealed the emergence of the charge loop current (cLC) order near the bond order (BO) phase. However, the origin of the cLC and its relation to other phases have been uncovered. Here, we discover a novel mechanism of the cLC state, by focusing on the BO phase common in kagome metals. The BO fluctuations in metals mediate the odd-parity particle-hole condensation, which drives the topological charge-current. This state is further stabilized by the finite electron-phonon coupling and the off-site Coulomb interaction. Furthermore, it is worth noting that the predicted cLC+BO phase gives rise to the Z_3 -nematic state in addition to the giant anomalous Hall effect. The present theory predicts the close relationship between the cLC, the BO, and the nematicity, which is significant to understand the cascade of quantum electron states in kagome metals.

Recent discovery of the kagome-lattice metal AV_3Sb_5 (A=K, Rb, Cs) shown in Fig. 1 (a) has opened the way to study the unique physics of geometrically frustrated metals with strong correlation [1–5]. In CsV_3Sb_5 , formation of the 2×2 Star-of-David or Tri-Hexagonal density wave (DW) was detected by scanning tunneling microscopy (STM) at $T \approx 90$ K at ambient pressure [6, 7]. It is presumably the triple- q ($3Q$) bond order (BO) shown in Fig. 1 (b), which is the even-parity modulation in the hopping integral δt_{ij}^b (=real) [8–13]. Inside the BO state ($T < T_{BO}$), the superconducting (SC) state emerges at $T_{SC} \approx 1 \sim 3$ K, while it increases to 8 K near the BO endpoint under $P \approx 3$ GPa [3–5]. Thus, the SC in kagome metals would be affected by the BO fluctuations [13].

More recently, the non-trivial time reversal symmetry breaking (TRSB) order at T_{TRSB} attracts considerable attention. The magneto-chiral anisotropy observed by STM [6, 14] strongly indicates the emergence of the chiral charge-loop-current (cLC) inside the BO phase. The Kerr rotation measurements suggest the appearance of the TRSB state at $T \sim T_{BO}$. On the other hand, the TRSB amplitude grows prominent at $T \approx 35$ K $< T_{BO}$ according to the muon spin relaxation (μ SR) studies [15–17] and the field-tuned chiral transport study [14]. The chiral cLC is driven by the additional odd-parity hopping integral δt_{ij}^c (=imaginary), and the accompanied topological charge-current [18] give the giant anomalous Hall effect (AHE) below $T \approx 35$ K [19, 20]. The correlation driven topological phase in kagome metals is very unique, and its mechanism should be revealed.

The cascade of rich quantum phases in kagome metals gives rise to various exotic electronic states. A notable example is the emergent nematic (C_2) order inside the BO and the cLC phases, which is clearly observed by the elastoresistance, [21] the scanning birefringence [17], and the STM [7] studies. In addition, nematic SC states have been reported [22, 23]. Thus, kagome metals provide a promising platform for exploring the interplay between the electron correlations and the topology.

Microscopically, the BO and the cLC are the non-local particle-hole (ph) condensation [8–13, 24–36]. Thus, the emergence of the BO/cLC indicates the existence of the large non-local effective interaction in kagome metals. It is given by the off-site Coulomb interaction V within the mean-field approximation (MFA) [10, 11, 37, 38], while the necessary model parameters are severe. Recently, sizable off-site interaction is found to be induced by the beyond-MFA effects [32–36], and the realized BO fluctuations mediate non-BCS SC states in Kagome metals [13] and other strongly correlated metals [27–32, 35]. Now, it is interesting to investigate the BO-fluctuation-mediated cLC state because this idea would lead to a unified understanding of the cascade of rich quantum phases.

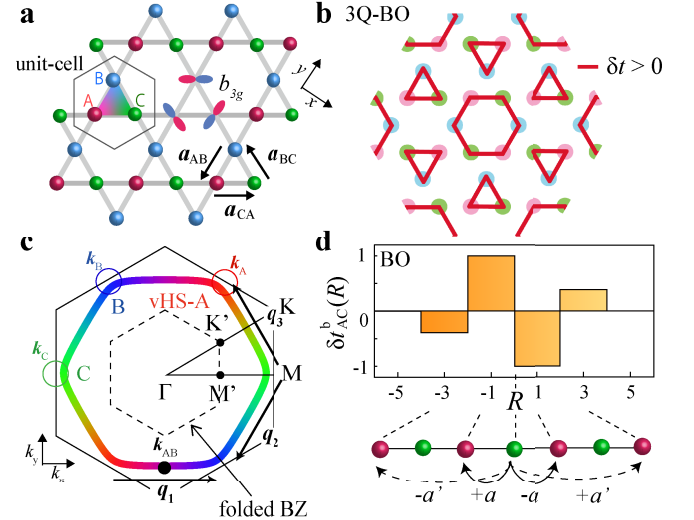


FIG. 1: (a) Kagome-lattice structure composed of the sublattices A, B and C. (b) $3Q$ Tri-Hexagonal BO state. (c) FS at $n = 0.875$ with the nesting vectors q_1, q_2, q_3 . (d) Bond-order fluctuation along A-C direction in real space; $\delta t_{AC}^b(R)$.

In this paper, we propose a cLC mechanism driven by the developed BO fluctuations in kagome metals. It is

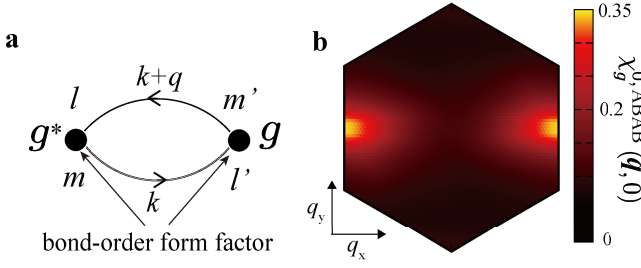


FIG. 2: (a) Expression of $\chi_g^{0,lmml'}$ (q). (b) q -dependence of $\chi_g^{0,ABAB}(\mathbf{q}, 0)$.

revealed that the quantum BO fluctuations in metals mediate the cLC order parameter (=imaginary δt_{ij}^c). This cLC mechanism is universal because it is irrelevant to the origin of the BO. Furthermore, we discover that the coexistence of the BO and the cLC order give rise to the novel Z_3 nematicity along the three lattice directions reported in Refs. [7, 17, 21]. The present theory reveals the close relationship between the cLC, BO, nematicity and SC state, which is significant to understand the unsolved quantum phase transitions in kagome metals.

Here, we introduce the kagome-lattice tight-binding model with b_{3g} -orbitals of the vanadium sites (A,B,C) shown in Fig. 1 (a). The kinetic term is given by $\hat{H}_0 = \sum_{\mathbf{k}, l, m, \sigma} h_{lm}^0(\mathbf{k}) c_{\mathbf{k}, l, \sigma}^\dagger c_{\mathbf{k}, m, \sigma}$, where l, m denote the sublattices A, B, C, and $h_{lm}^0(\mathbf{k}) (= h_{ml}^0(\mathbf{k})^*)$ is the Fourier transform of the nearest-neighbor hopping integral $t (= 0.5\text{eV})$. Here, we set the unit of energy eV. The temperature is set to $T = 0.05$ in the numerical calculation. The Fermi surface (FS) at $n = 0.875$ per site is shown in Fig. 1 (c). The FS is close to the three van-Hove singular (vHS) points ($\mathbf{k}_A, \mathbf{k}_B, \mathbf{k}_C$), each of which is composed of a single b_{3g} -orbital. This simple three-orbital model well captures the main pure-type FS in kagome metals [6, 39–43]. The wavevectors of the BO correspond to the inter-sublattice nesting vectors \mathbf{q}_n ($n = 1, 2, 3$) in Fig. 1 (c). (The equivalent square lattice kagome model is convenient for the numerical study; see SM A [44].)

Based on the kagome-lattice Hubbard model with on-site U , the experimental BO at $\mathbf{q} = \mathbf{q}_n$ is derived from the paramagnon-interference mechanism [13]. Figure 1 (d) shows the corresponding hopping modulation along the A-C direction due to the BO, $\delta t_{AC}^b(R) \equiv \delta t_{iA, jC}^b$, where $R \equiv \mathbf{a}_{AC} \cdot (\mathbf{r}_i^A - \mathbf{r}_j^C)$ is odd-integer. The obtained BO is mainly given by the nearest-neighbor components, and it exhibits the staggered pattern $\delta t_{AC}^b(R) = -\delta t_{AC}^b(-R)$.

The Fourier transform of the BO modulation, δt_{ij}^b , gives the even-parity BO form factor $g_{\mathbf{q}}^{lm}(\mathbf{k})$: [36, 45]:

$$g_{\mathbf{q}}^{lm}(\mathbf{k}) = \frac{1}{N} \sum_i^{\text{sub-l}} \sum_j^{\text{sub-m}} \delta t_{ij}^b e^{i\mathbf{k} \cdot (\mathbf{r}_i - \mathbf{r}_j)} e^{-i\mathbf{q} \cdot \mathbf{r}_j}. \quad (1)$$

where \mathbf{q} is the wavevector of the BO. Here, we use the BO form factor derived in Ref. [13].

Below, we study the cLC mechanism due to the BO fluctuations. For this purpose, we introduce the following effective BO interaction to derive the BO susceptibility:

$$\hat{H}_{\text{int}} = -\frac{1}{N} \sum_{\mathbf{q}} \frac{v}{2} \hat{O}_{\mathbf{q}}^g \hat{O}_{-\mathbf{q}}^g, \quad (2)$$

where $\hat{O}_{\mathbf{q}}^g \equiv \sum_{\mathbf{k}, l, m, \sigma} g_{\mathbf{q}}^{lm}(\mathbf{k}) c_{\mathbf{k}+\mathbf{q}, l, \sigma}^\dagger c_{\mathbf{k}, m, \sigma}$ is the BO operator [36, 45, 46]. Here, v is the effective interaction, and the form factor $g_{\mathbf{q}}^{lm}(\mathbf{k})$ is normalized as $\max_{\mathbf{k}, l, m} |g_{\mathbf{q}}^{lm}(\mathbf{k})| = 1$ at each \mathbf{q} . The interaction (2) would originate from the combination of (i) the paramagnon-interference due to on-site U [13], (ii) the Fock term of off-site V [11], and (iii) the bond-stretching phonon [47]. As for (iii), $g_{\mathbf{q}}^{lm}(\mathbf{k})$ is given by the hopping modulation due to the stretching mode and $v = 2\eta^2/\omega_D$, where η is the electron-phonon coupling constant and ω_D is the phonon energy at $\mathbf{q} \approx \mathbf{q}_n$. As for (ii), $v = 2V$ as we explain in the SM B [44]. Thus, the effective interaction (2) is general. Possible driving force of the BO has been discussed experimentally [48, 49].

Next, we calculate the BO susceptibility per spin given as $\chi_g(\mathbf{q}, \omega_l) \equiv \frac{1}{2} \int_0^\beta d\tau \langle \hat{O}_{\mathbf{q}}^g(\tau) \hat{O}_{-\mathbf{q}}^g(0) \rangle e^{i\omega_l \tau}$, where ω_l is boson Matsubara frequency. By applying the random-phase approximation (RPA), $\chi_g(\mathbf{q}, \omega_l)$ is obtained as

$$\chi_g(q) = \chi_g^0(q)/(1 - v\chi_g^0(q)), \quad (3)$$

where the notation $q \equiv (\mathbf{q}, \omega_l)$ is used. The BO irreducible susceptibility $\chi_g^0(q)$ is given by [36, 45]

$$\begin{aligned} \chi_g^0(q) &= \sum_{lmml'} \chi_g^{0,lmml'}(q), \\ \chi_g^{0,lmml'}(q, \omega_l) &= \frac{T}{N} \sum_{\mathbf{k}, \epsilon_n} g_{\mathbf{q}}^{lm}(\mathbf{k})^* G_{lm'}(\mathbf{k} + \mathbf{q}, \epsilon_n + \omega_l) \\ &\quad \times G_{l'm}(\mathbf{k}, \epsilon_n) g_{\mathbf{q}}^{m'l'}(\mathbf{k}), \end{aligned} \quad (4)$$

where ϵ_n is a fermion Matsubara frequency. Its diagrammatic expression and the numerical result are shown in Figs. 2 (a) and (b), respectively. Note that the spin susceptibility is not changed by v .

Now, we explain the BO fluctuation-mediated cLC order. Although the cLC instability is smaller than others in the MFA as shown in SM B [44], its instability is strongly magnified by the beyond-MFA effects. In two-dimensional metals, in general, spin- or charge-channel fluctuations induce prominent beyond-MFA effects that is called the vertex corrections [27–36]. As revealed in Ref. [50], the Maki-Thompson (MT) vertex correction due to the spin-fluctuations induces the cLC state in a frustrated Hubbard model based on the functional-renormalization-group theory. In kagome metals, instead of spin fluctuations, BO fluctuations are expected to mediate the cLC state. Therefore, we solve the following linearized DW equation [32, 50, 51] by considering the

BO fluctuations in Eq. (3), and obtain the odd-parity cLC solution $\delta t_{ij}^c = -\delta t_{ji}^c$:

$$\lambda_{\mathbf{q}} f_{\mathbf{q}}^L(k) = -\frac{T}{N} \sum_{p, M_1, M_2} I_{\mathbf{q}}^{L, M_1}(k, p) \times \{G(p)G(p+\mathbf{q})\}^{M_1, M_2} f_{\mathbf{q}}^{M_2}(p), \quad (6)$$

where $I_{\mathbf{q}}^{L, M}(k, p)$ is the electron-hole pairing interaction due to the MT term. $L \equiv (l, l')$ and M_i represent the pair of sublattice indices. $\lambda_{\mathbf{q}}$ is the eigenvalue that represents the instability of the DW at wavevector \mathbf{q} , and $\max_{\mathbf{q}}\{\lambda_{\mathbf{q}}\}$ is unity at the transition temperature. $f_{\mathbf{q}}^L(k)$ is the Hermitian form factor that is proportional to the ph condensation or, equivalently, the symmetry breaking component in the self-energy. [26, 27, 31, 32, 52].

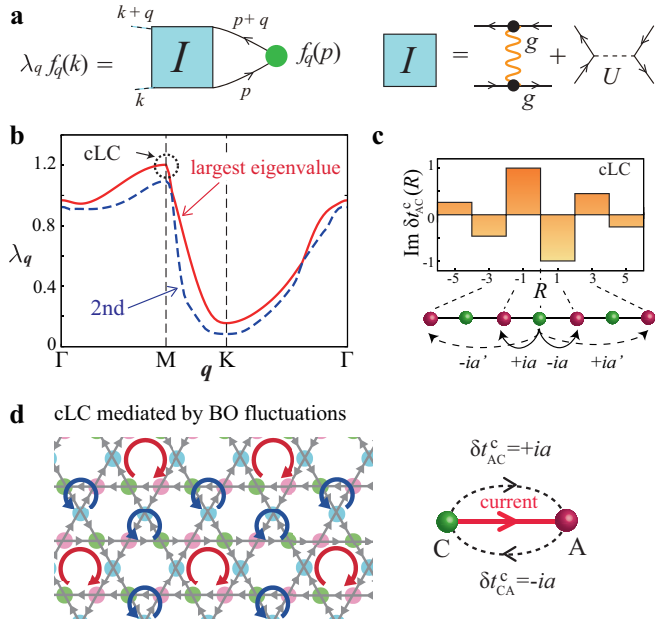


FIG. 3: (a) DW equation due to the single exchange term of χ_g . (b) \mathbf{q} -dependent eigenvalue of the DW equation. Red-solid (blue-dashed) line denotes the largest (second-largest) eigenvalue, and both show peaks at $\mathbf{q} = \mathbf{q}_n$. (c) Imaginary hopping modulation $\text{Im}\delta t_{AC}^c(R)$. Its triple- \mathbf{q} order gives the cLC pattern in (d). One can check that the clock-wise (anti-clock-wise) loop currents on hexagons (triangles) in (d) are inverted and moved by \mathbf{a}_{AC} under the sign change of $f_{\mathbf{q}_3}^{AC}$.

The kernel function due to the single exchange of the BO fluctuations, $I_{BO} \propto \chi_g$, is given as

$$I_{BO, \mathbf{q}}^{ll', mm'}(k, p) = g_{\mathbf{p}-\mathbf{k}}^{m'l'}(\mathbf{k}) y v^2 (v^{-1} + \chi_g(k-p)) \times g_{\mathbf{k}-\mathbf{p}}^{lm}(\mathbf{p} + \mathbf{q}), \quad (7)$$

which is diagrammatically expressed in Fig. 3 (a). In addition, we include the Hartree term due to U , $I_U^{ll', mm'} = U \delta_{l, l'} \delta_{m, m'} \delta_{l, m}$. This term leads to the suppression of the net charge order, while the BO and cLC are not suppressed at all. Here, the kernel function is given by

$I = I_{BO} + I_U$, and we set $v = 1.53$ and $U = 1.27$. Note that the coefficient y in Eq. (7) depends on the origin of the BO: $y = 1/2$ in the phonon mechanism, while $y = 2$ in the Fock term of off-site V because both charge- and three spin-channel BO fluctuations develop, as explained in SM B [44]. $y \gg 1$ can be realized in the paramagnon-interference mechanism [13]. Because we are interested in a general argument, we simply set $y = 1$ below.

Figure 3 (b) shows the \mathbf{q} -dependence of the largest (second-largest) eigenvalue $\lambda_{\mathbf{q}}$ by solving the DW equation in red solid (blue dashed) line. The largest eigenvalue exhibits the maximum value at $\mathbf{q} = \mathbf{q}_n$ ($n = 1, 2, 3$), and its form factor is odd-parity: $f_{\mathbf{q}}^{lm}(\mathbf{k} - \mathbf{q}/2) = -f_{\mathbf{q}}^{ml}(-\mathbf{k} - \mathbf{q}/2)$. Then, the corresponding real-space hopping modulation is odd-parity $\delta t_{ij}^c = -\delta t_{ji}^c$ and pure imaginary when δt_{ij}^c is Hermitian. The obtained $\delta t_{AC}^c(R) \equiv \delta t_{i_A j_C}^c$ for the cLC at $\mathbf{q} = \mathbf{q}_3$ along the A-C direction is shown in Fig. 3 (c), where $R \equiv \mathbf{a}_{CA} \cdot (\mathbf{r}_i^C - \mathbf{r}_j^A)$ is odd-integer. In addition, the odd-parity relation $\delta t_{AC}^c(R) = -\delta t_{CA}^c(-R)$ is verified. The obtained charge loop current pattern for the $3Q$ state is depicted in Fig. 3 (d).

Note that the second-largest eigenvalue at $\mathbf{q} = \mathbf{q}_n$ in Fig. 3 (b) corresponds to the charge order ($n_A \neq n_B$), originating from the flatness of the FS between two vHS points in this simplified model in Fig. 1 (c). This instability is suppressed by U due to its Hartree term. Also, we discuss that the Aslamazov-Larkin (AL) term is unimportant in the SM C [44].

Here, we discuss why the cLC order is mediated by the BO fluctuations. Figures 4 (a) and (b) show the first- and the second-order scattering processes derived from the DW equation (6) at $\mathbf{q} = \mathbf{q}_3$, respectively. The former umklapp term gives the repulsive interaction that leads to $f_{\mathbf{q}_3}^{AC} = -f_{\mathbf{q}_3}^{CA}$, and the latter backward term gives the attraction among the same $f_{\mathbf{q}_3}^{lm}$. Thus, both interactions cooperatively induce the odd-parity current order form factor in Fig. 3 (c). The infinite series of such ladder diagrams are calculated by solving Eq. (6), and the obtained v -dependence of the cLC eigenvalue is shown in Fig. 4 (c). A schematic BO+cLC phase diagram derived from the present theory is depicted in Fig. 4 (d). This phase diagram is reminiscent of that of the d -wave SC state around the antiferromagnetic endpoint.

In the next stage, we discuss the electronic nematic states due to the coexistence of the BO (δt_{ij}^b) in Fig. 1 (b) and the cLC order (δt_{ij}^c) in Fig. 3 (d). Here, we set $|\delta t_{ij}^b| = |\delta t_{ij}^c| = 0.05$. In Fig. 5 (a), the hexagonal loop current pattern in the cLC coincides with the hexagonal bond pattern in the BO. Its folded FS has C_6 symmetry as shown in Fig. 5 (b). In Fig. 5 (c), we shift the cLC pattern by \mathbf{a}_{BA} . Then, the center of C_6 symmetry in the BO and that of the cLC do not coincide, and the realized FS has C_2 symmetry as depicted in Fig. 5 (d). This nematicity is rotated by 120 (240) degrees by displacing

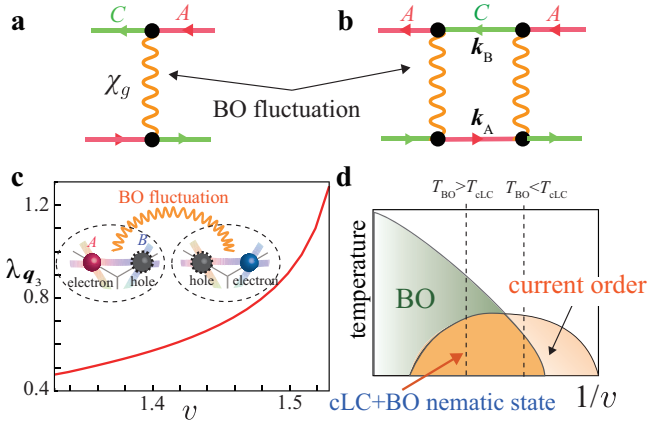


FIG. 4: (a) The first- and (b) the second-order scattering processes with respect to χ_g . The repulsion (attraction) due to the odd- (even-) order terms cause the cLC ph pairs. (c) v -dependence of the eigenvalue of cLC λ_{q_3} . (d) Schematic phase diagram predicted in the present study. The cLC is mediated by the BO fluctuations near the BO-endpoint.

the cLC pattern by \mathbf{a}_{CA} (\mathbf{a}_{BC}). Thus, the coexistence of the BO and cLC leads to the Z_3 nematic order. This is consistent with the nematic transition at $T_{nem} \approx 35$ K observed by the nematic susceptibility measurement [21].

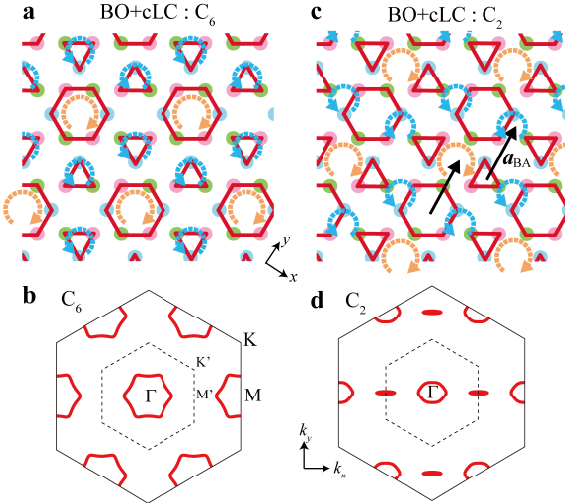


FIG. 5: (a) C_6 -symmetric BO+cLC state in real space and (b) its folded FS. The folded Brillouin zone (BZ) is shown by dotted lines. (c) Nematic BO+cLC state with the director parallel to \mathbf{a}_{BA} and (d) its nematic FS. Here, we changed the sign of $f_{q_1}^{AB}$ in (a). The nematic state parallel to \mathbf{a}_{tm} appears by changing the sign of $f_{q_n}^{lm}$ in (a). Thus, the Z_3 nematic state is realized. Here, we use large $|\delta t_{ij}^{b,c}|$ ($= 0.05$) to exaggerate the nematicity.

Here, we briefly discuss the realized phase diagram based on the Ginzburg-Landau (GL) free energy. (i) When the BO solely occurs, the $3Q$ BO state is more stable than the $1Q$ one due to the third-order GL term [12, 13, 53]. (ii) When the cLC order occurs inside the $3Q$

BO state ($T < T_{cLC} < T_{BO}$), the nematic BO+cLC state in Fig. 5 (c) is more stable than the hexagonal BO+cLC state (= Fig. 5 (a)) and the $(1Q \text{ cLC})+(3Q \text{ BO})$ state due to the third-order GL term, as we discuss in the SM D [44]. (iii) When the cLC solely occurs, the third-order GL term vanishes, and the $3Q$ ($1Q$) cLC order emerges when $r \equiv d_{2,b}/2d_{2,a} < 1$ ($r > 1$), where $d_{2,a}, d_{2,b}$ are the fourth order GL parameters [44]. Note that the $1Q$ cLC order corresponds to a nematic state.

We note that the nematic state is also caused by the $3Q$ state composed of the three-dimensional (3D) BO at \mathbf{q}_n^{3D} with $q_{1,z}^{3D} = q_{2,z}^{3D} = \pi$ and $q_{3,z}^{3D} = 0$, as discussed in Ref. [12]: This nematic 3D-BO state is different from the present TRSB nematic BO+cLC state. These two different nematic states would be realized at different temperatures.

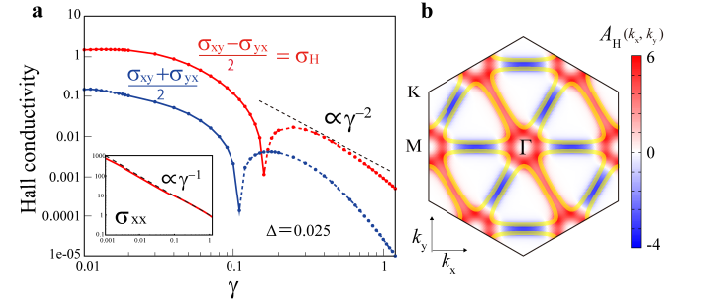


FIG. 6: (a) Anomalous Hall conductivity in the nematic BO+cLC state ($|\delta t_{ij}^{b,c}| = 0.025$) as a function of $\gamma \propto \tau^{-1}$. The full (broken) line represents the positive (negative) value. The obtained $\sigma_H = 1.5$ at $\gamma = 0.01$ is reduced to $\sigma_H = 1.1$ by dropping the BO. (b) $A_H(\mathbf{k})$ at $\gamma = 0.05$: $\frac{1}{N} \sum_{\mathbf{k}} A_H(\mathbf{k}) = \sigma_H$.

Finally, we discuss the transport phenomena that originate from the cLC [18, 54]. Using the general expression of the intrinsic conductivity [55–59], we calculate the Hall conductivity (σ_{xy} and σ_{yx}) due to the Fermi-surface contribution in the BO+cLC state. The expression is $\sigma_{\mu\nu} = \frac{1}{N} \sum_{\mathbf{k}} A_{\mu\nu}(\mathbf{k})$, where $A_{\mu\nu}(\mathbf{k}) = \frac{e^2}{\hbar} \frac{1}{\pi} \text{Tr} \{ \hat{v}_{\mathbf{k},\mu} \hat{G}_{\mathbf{k}}(i\gamma) \hat{v}_{\mathbf{k},\nu} \hat{G}_{\mathbf{k}}(-i\gamma) \}$. Here, $\hat{G}_{\mathbf{k}}(\epsilon) = ((\epsilon + \mu)\hat{1} - \hat{h}_{\mathbf{k}})^{-1}$ is the Green function matrix, where $\hat{h}_{\mathbf{k}}$ is the 12×12 tight-binding model with the $3Q$ BO and cLC order, and $\hat{v}_{\mathbf{k},\mu} = d\hat{h}_{\mathbf{k}}/dk_{\mu}$ is the velocity operator. γ (> 0) is the quasiparticle damping that is given by the imaginary part of the self-energy. We set $n = 0.895$ and $|\delta t_{ij}^b| = |\delta t_{ij}^c| = 0.025$, where the band hybridization gap due to the BO+cLC order is about $\Delta \approx 2\sqrt{|\delta t_{ij}^b|^2 + |\delta t_{ij}^c|^2} = 0.07$.

Figure 6 (a) shows the obtained conductivities in the nematic BO+cLC state, in the unit of $\frac{e^2}{\hbar}$ ($= 2.4 \times 10^{-4} \Omega^{-1}$). When $\gamma \ll \Delta$, the Hall conductivity $\sigma_H \equiv \frac{1}{2}(\sigma_{xy} - \sigma_{yx})$ is almost constant, and its magnitude is proportional to $|\delta t_{ij}^c|$. When $\gamma \gg \Delta$, in contrast, σ_H decreases with γ in proportion to γ^{-2} . This crossover

behavior is universal in the intrinsic Hall effect, which was first revealed in heavy fermion systems [55], and found to be universal in later studies [56–60]. Note that $\frac{1}{2}(\sigma_{xy} + \sigma_{yx})$ is nonzero in the nematic state. To understand the origin of the intrinsic Hall effect, we plot $A_H(\mathbf{k}) \equiv (A_{xy}(\mathbf{k}) - A_{yx}(\mathbf{k}))/2$ at $\gamma = 0.05$ in Fig. 6 (b): It shows a large positive value mainly around the vHS points, due to the band-hybridization induced by the cLC order. The obtained $\sigma_H \sim 1$ corresponds to $4 \times 10^3 \Omega^{-1} \text{cm}^{-1}$ because the interlayer spacing is $\sim 0.6 \text{nm}$. Thus, giant AHE $\sigma_H \sim 10^2 \Omega^{-1} \text{cm}^{-1}$ reported in Refs. [19, 20] is understood in this theory.

In summary, we proposed a cLC mechanism mediated by the BO fluctuations in kagome metals. This mechanism is universal because it is independent of the origin of the BO. Furthermore, we revealed that novel Z_3 nematicity emerges under the coexistence of the cLC and the BO reported in Refs. [7, 17, 21] in addition to the giant AHE [19, 20]. This theory presents a promising scenario for understanding the BO, the cLC and the nematicity in kagome metals in a unified way.

We are grateful to S. Onari, A. Ogawa, Y. Matsuda, T. Shibauchi, K. Hashimoto, and T. Asaba for fruitful discussions. This study has been supported by Grants-in-Aid for Scientific Research from MEXT of Japan (JP18H01175, JP20K03858, JP20K22328, JP22K14003), and by the Quantum Liquid Crystal No. JP19H05825 KAKENHI on Innovative Areas from JSPS of Japan.

-
- [1] B. R. Ortiz, L. C. Gomes, J. R. Morey, M. Winiarski, M. Bordelon, J. S. Mangum, I. W. H. Oswald, J. A. Rodriguez-Rivera, J. R. Neilson, S. D. Wilson, E. Ertekin, T. M. McQueen, and E. S. Toberer, *New kagome prototype materials: discovery of KV_3Sb_5 , RbV_3Sb_5 , and CsV_3Sb_5* , Phys. Rev. Materials **3**, 094407 (2019).
- [2] B. R. Ortiz, S. M. L. Teicher, Y. Hu, J. L. Zuo, P. M. Sarte, E. C. Schueller, A. M. M. Abeykoon, M. J. Krogstad, S. Rosenkranz, R. Osborn, R. Seshadri, L. Balents, J. He, and S. D. Wilson, *CsV_3Sb_5 : A Z_2 Topological Kagome Metal with a Superconducting Ground State*, Phys. Rev. Lett. **125**, 247002 (2020).
- [3] F. H. Yu, D. H. Ma, W. Z. Zhuo, S. Q. Liu, X. K. Wen, B. Lei, J. J. Ying, and X. H. Chen, *Unusual competition of superconductivity and charge-density-wave state in a compressed topological kagome metal*, Nat. Commun. **12**, 3645 (2021).
- [4] K. Y. Chen, N. N. Wang, Q. W. Yin, Y. H. Gu, K. Jiang, Z. J. Tu, C. S. Gong, Y. Uwatoko, J. P. Sun, H. C. Lei, J. P. Hu, and J.-G. Cheng, *Double Superconducting Dome and Triple Enhancement of T_c in the Kagome Superconductor CsV_3Sb_5 under High Pressure*, Phys. Rev. Lett. **126**, 247001 (2021).
- [5] B. R. Ortiz, P. M. Sarte, E. M. Kenney, M. J. Graf, S. M. L. Teicher, R. Seshadri, and S. D. Wilson, *Superconductivity in the Z_2 kagome metal KV_3Sb_5* , Phys. Rev. Materials **5**, 034801 (2021).
- [6] Y.-X. Jiang, J.-X. Yin, M. M. Denner, N. Shumiya, B. R. Ortiz, G. Xu, Z. Guguchia, J. He, M. S. Hossain, X. Liu, J. Ruff, L. Kautzsch, S. S. Zhang, G. Chang, I. Belopolski, Q. Zhang, T. A. Cochran, D. Multer, M. Litskevich, Z.-J. Cheng, X. P. Yang, Z. Wang, R. Thomale, T. Neupert, S. D. Wilson, and M. Z. Hasan, *Unconventional chiral charge order in kagome superconductor KV_3Sb_5* , Nat. Mater. **20**, 1353 (2021).
- [7] H. Li, H. Zhao, B. R. Ortiz, T. Park, M. Ye, L. Balents, Z. Wang, S. D. Wilson, and I. Zeljkovic, *Rotation symmetry breaking in the normal state of a kagome superconductor KV_3Sb_5* , Nat. Phys. **18**, 265 (2022).
- [8] M. L. Kiesel, C. Platt, and R. Thomale, *Unconventional Fermi Surface Instabilities in the Kagome Hubbard Model*, Phys. Rev. Lett. **110**, 126405 (2013).
- [9] W.-S. Wang, Z.-Z. Li, Y.-Y. Xiang, and Q.-H. Wang, *Competing electronic orders on kagome lattices at van Hove filling*, Phys. Rev. B **87**, 115135 (2013).
- [10] X. Wu, T. Schwemmer, T. Müller, A. Consiglio, G. Sangiovanni, D. Di Sante, Y. Iqbal, W. Hanke, A. P. Schnyder, M. M. Denner, M. H. Fischer, T. Neupert, and R. Thomale, *Nature of Unconventional Pairing in the Kagome Superconductors AV_3Sb_5 ($A = K, Rb, Cs$)*, Phys. Rev. Lett. **127**, 177001 (2021).
- [11] M. M. Denner, R. Thomale, and T. Neupert, *Analysis of Charge Order in the Kagome Metal AV_3Sb_5 ($A = K, Rb, Cs$)*, Phys. Rev. Lett. **127**, 217601 (2021).
- [12] T. Park, M. Ye, and L. Balents, *Electronic instabilities of kagome metals: Saddle points and Landau theory*, Phys. Rev. B **104**, 035142 (2021).
- [13] R. Tazai, Y. Yamakawa, S. Onari, and H. Kontani, *Mechanism of exotic density-wave and beyond-Migdal unconventional superconductivity in kagome metal AV_3Sb_5 ($A = K, Rb, Cs$)*, Sci. Adv. **8**, eabb4108 (2022).
- [14] C. Guo, C. Putzke, S. Konyzheva, X. Huang, M. Gutierrez-Amigo, I. Errea, D. Chen, M. G. Vergniory, C. Felser, M. H. Fischer, T. Neupert, and P. J. W. Moll, *Field-tuned chiral transport in charge-ordered CsV_3Sb_5* , arXiv:2203.09593.
- [15] L. Yu, C. Wang, Y. Zhang, M. Sander, S. Ni, Z. Lu, S. Ma, Z. Wang, Z. Zhao, H. Chen, K. Jiang, Y. Zhang, H. Yang, F. Zhou, X. Dong, S. L. Johnson, M. J. Graf, J. Hu, H.-J. Gao, and Z. Zhao, *Evidence of a hidden flux phase in the topological kagome metal CsV_3Sb_5* , arXiv:2107.10714.
- [16] C. Mielke, D. Das, J.-X. Yin, H. Liu, R. Gupta, Y.-X. Jiang, M. Medarde, X. Wu, H. C. Lei, J. Chang, P. Dai, Q. Si, H. Miao, R. Thomale, T. Neupert, Y. Shi, R. Khasanov, M. Z. Hasan, H. Luetkens, and Z. Guguchia, *Time-reversal symmetry-breaking charge order in a kagome superconductor*, Nature **602**, 245 (2022).
- [17] Y. Xu, Z. Ni, Y. Liu, B. R. Ortiz, S. D. Wilson, B. Yan, L. Balents, and L. Wu, *Universal three-state nematicity and magneto-optical Kerr effect in the charge density waves in AV_3Sb_5 ($A=Cs, Rb, K$)*, arXiv:2204.10116.
- [18] F. D. M. Haldane, *Model for a Quantum Hall Effect without Landau Levels: Condensed-Matter Realization of the "Parity Anomaly"*, Phys. Rev. Lett. **61**, 2015 (1988).
- [19] S.-Y. Yang, Y. Wang, B. R. Ortiz, D. Liu, J. Gayles, E. Derunova, R. Gonzalez-Hernandez, L. Šmejkal, Y. Chen, S. S. P. Parkin, S. D. Wilson, E. S. Toberer, T. McQueen, and M. N. Ali, *Giant, unconventional anomalous Hall effect in the metallic frustrated magnet candidate, KV_3Sb_5* , Sci. Adv. **6**, eabb6003 (2020).

- [20] F. H. Yu, T. Wu, Z. Y. Wang, B. Lei, W. Z. Zhuo, J. J. Ying, and X. H. Chen, *Concurrence of anomalous Hall effect and charge density wave in a superconducting topological kagome metal*, Phys. Rev. B **104**, L041103 (2021).
- [21] L. Nie, K. Sun, W. Ma, D. Song, L. Zheng, Z. Liang, P. Wu, F. Yu, J. Li, M. Shan, D. Zhao, S. Li, B. Kang, Z. Wu, Y. Zhou, K. Liu, Z. Xiang, J. Ying, Z. Wang, T. Wu, and X. Chen, *Charge-density-wave-driven electronic nematicity in a kagome superconductor*, Nature **604**, 59 (2022).
- [22] S. Ni, S. Ma, Y. Zhang, J. Yuan, H. Yang, Z. Lu, N. Wang, J. Sun, Z. Zhao, D. Li, S. Liu, H. Zhang, H. Chen, K. Jin, J. Cheng, L. Yu, F. Zhou, X. Dong, J. Hu, H.-J. Gao, and Z. Zhao, *Anisotropic Superconducting Properties of Kagome Metal CsV_3Sb_5* , Chin. Phys. Lett. **38**, 057403 (2021).
- [23] Y. Xiang, Q. Li, Y. Li, W. Xie, H. Yang, Z. Wang, Y. Yao, and H.-H. Wen, *Twofold symmetry of c -axis resistivity in topological kagome superconductor CsV_3Sb_5 with in-plane rotating magnetic field*, Nat. Commun. **12**, 6727 (2021).
- [24] E. Fradkin and S. A. Kivelson, *Ineluctable complexity*, Nat. Phys. **8**, 864 (2012).
- [25] J. C. S. Davis and D.-H. Lee, *Concepts relating magnetic interactions, intertwined electronic orders, and strongly correlated superconductivity*, Proc. Natl. Acad. Sci. U.S.A. **110**, 17623 (2013).
- [26] H. Kontani, T. Saito, and S. Onari, *Origin of orthorhombic transition, magnetic transition, and shear-modulus softening in iron pnictide superconductors: Analysis based on the orbital fluctuations theory*, Phys. Rev. B **84**, 024528 (2011).
- [27] S. Onari and H. Kontani, *Self-consistent Vertex Correction Analysis for Iron-based Superconductors: Mechanism of Coulomb Interaction-Driven Orbital Fluctuations*, Phys. Rev. Lett. **109**, 137001 (2012).
- [28] M. Tsuchiizu, Y. Ohno, S. Onari, and H. Kontani, *Orbital Nematic Instability in the Two-Orbital Hubbard Model: Renormalization-Group + Constrained RPA Analysis*, Phys. Rev. Lett. **111**, 057003 (2013).
- [29] M. Tsuchiizu, K. Kawaguchi, Y. Yamakawa, and H. Kontani, *Multistage electronic nematic transitions in cuprate superconductors: A functional-renormalization-group analysis*, Phys. Rev. B **97**, 165131 (2018).
- [30] Y. Yamakawa and H. Kontani, *Spin-Fluctuation-Driven Nematic Charge-Density Wave in Cuprate Superconductors: Impact of Aslamazov-Larkin Vertex Corrections*, Phys. Rev. Lett. **114**, 257001 (2015).
- [31] Y. Yamakawa, S. Onari, and H. Kontani, *Nematicity and Magnetism in $FeSe$ and Other Families of Fe-Based Superconductors*, Phys. Rev. X **6**, 021032 (2016).
- [32] S. Onari, Y. Yamakawa, and H. Kontani, *Sign-Reversing Orbital Polarization in the Nematic Phase of $FeSe$ due to the C_2 Symmetry Breaking in the Self-Energy*, Phys. Rev. Lett. **116**, 227001 (2016).
- [33] A. V. Chubukov, M. Khodas, and R. M. Fernandes, *Magnetism, Superconductivity, and Spontaneous Orbital Order in Iron-Based Superconductors: Which Comes First and Why?*, Phys. Rev. X **6**, 041045 (2016).
- [34] R. M. Fernandes, P. P. Orth, and J. Schmalian, *Intertwined Vestigial Order in Quantum Materials: Nematicity and Beyond*, Annu. Rev. Condens. Matter Phys. **10**, 133 (2019).
- [35] S. Onari and H. Kontani, *$SU(4)$ Valley+Spin Fluctuation Interference Mechanism for Nematic Order in Magic-Angle Twisted Bilayer Graphene: The Impact of Vertex Corrections*, Phys. Rev. Lett. **128**, 066401 (2022).
- [36] H. Kontani, Y. Yamakawa, R. Tazai, and S. Onari, *Odd-parity spin-loop-current order mediated by transverse spin fluctuations in cuprates and related electron systems*, Phys. Rev. Research **3**, 013127 (2021).
- [37] C. M. Varma, *Non-Fermi-liquid states and pairing instability of a general model of copper oxide metals*, Phys. Rev. B **55**, 14554 (1997).
- [38] A. A. Nersesyan, G. I. Japaridze, and I. G. Kimeridze, *Low-temperature magnetic properties of a two-dimensional spin nematic state*, J. Phys.: Condens. Matter **3**, 3353 (1991).
- [39] Y. Hu, X. Wu, B. R. Ortiz, S. Ju, X. Han, J. Ma, N. C. Plumb, M. Radovic, R. Thomale, S. D. Wilson, A. P. Schnyder, and M. Shi, *Rich nature of Van Hove singularities in Kagome superconductor CsV_3Sb_5* , Nature **13**, 2220 (2022).
- [40] Y. Luo, S. Peng, S. M. L. Teicher, L. Huai, Y. Hu, B. R. Ortiz, Z. Wei, J. Shen, Z. Ou, B. Wang, Y. Miao, M. Guo, M. Shi, S. D. Wilson, and J.-F. He, *Distinct band reconstructions in kagome superconductor CsV_3Sb_5* , arXiv:2106.01248.
- [41] K. Nakayama, Y. Li, T. Kato, M. Liu, Z. Wang, T. Takahashi, Y. Yao, and T. Sato, *Multiple energy scales and anisotropic energy gap in the charge-density-wave phase of the kagome superconductor CsV_3Sb_5* , Phys. Rev. B **104**, L161112 (2021).
- [42] Z. Liu, N. Zhao, Q. Yin, C. Gong, Z. Tu, M. Li, W. Song, Z. Liu, D. Shen, Y. Huang, K. Liu, H. Lei, and S. Wang, *Charge-Density-Wave-Induced Bands Renormalization and Energy Gaps in a Kagome Superconductor RbV_3Sb_5* , Phys. Rev. X **11**, 041010 (2021).
- [43] Z. Wang, S. Ma, Y. Zhang, H. Yang, Z. Zhao, Y. Ou, Y. Zhu, S. Ni, Z. Lu, H. Chen, K. Jiang, L. Yu, Y. Zhang, X. Dong, J. Hu, H.-J. Gao, and Z. Zhao, *Distinctive momentum dependent charge-density-wave gap observed in CsV_3Sb_5 superconductor with topological Kagome lattice*, arXiv:2104.05556.
- [44] Supplementary Materials.
- [45] R. Tazai, Y. Yamakawa, M. Tsuchiizu, and H. Kontani, *d - and p -wave Quantum Liquid Crystal Orders in Cuprate Superconductors, κ -(BEDT-TTF) $_2X$, and Coupled Chain Hubbard Models: Functional-renormalization-group Analysis*, J. Phys. Soc. Jpn. **90**, 111012 (2021).
- [46] H. Kontani and S. Onari, *Orbital-Fluctuation-Mediated Superconductivity in Iron Pnictides: Analysis of the Five-Orbital Hubbard-Holstein Model*, Phys. Rev. Lett. **104**, 157001 (2010).
- [47] H. Tan, Y. Liu, Z. Wang, and B. Yan, *Charge Density Waves and Electronic Properties of Superconducting Kagome Metals*, Phys. Rev. Lett. **127**, 046401 (2021).
- [48] H. Li, T. T. Zhang, T. Yilmaz, Y. Y. Pai, C. E. Marvinney, A. Said, Q. W. Yin, C. S. Gong, Z. J. Tu, E. Vescovo, C. S. Nelson, R. G. Moore, S. Murakami, H. C. Lei, H. N. Lee, B. J. Lawrie, and H. Miao, *Observation of Unconventional Charge Density Wave without Acoustic Phonon Anomaly in Kagome Superconductors AV_3Sb_5 ($A = Rb, Cs$)*, Phys. Rev. X **11**, 031050 (2021).
- [49] Z. X. Wang, Q. Wu, Q. W. Yin, C. S. Gong, Z. J. Tu, T. Lin, Q. M. Liu, L. Y. Shi, S. J. Zhang, D. Wu, H. C. Lei, T. Dong, and N. L. Wang, *Unconventional charge density wave and photoinduced lattice symmetry change*

- in the kagome metal CsV_3Sb_5 probed by time-resolved spectroscopy, *Phys. Rev. B* **104**, 165110 (2021).
- [50] R. Tazai, Y. Yamakawa, and H. Kontani, *Emergence of charge loop current in the geometrically frustrated Hubbard model: A functional renormalization group study*, *Phys. Rev. B* **103**, L161112 (2021).
- [51] R. Tazai, S. Matsubara, Y. Yamakawa, S. Onari, and H. Kontani, *A Rigorous Formalism of Unconventional Symmetry Breaking in Fermi Liquid Theory and Its Application to Nematicity in FeSe*, arXiv:2205.02280.
- [52] S. Onari and H. Kontani, *Hidden antiferromagnetic order in Fe-based superconductor $BaFe_2As_2$ and $NaFeAs$ above T_S* , *Phys. Rev. Research* **2**, 042005(R) (2020).
- [53] T. Hirata, Y. Yamakawa, S. Onari, and H. Kontani, *Unconventional orbital charge density wave mechanism in the transition metal dichalcogenide $1T-TaS_2$* , *Phys. Rev. Research* **3**, L032053 (2021).
- [54] X. Feng, K. Jiang, Z. Wang, and J. Hu, *Chiral flux phase in the Kagome superconductor AV_3Sb_5* , *Sci. Bull.* **66**, 1384 (2021).
- [55] H. Kontani and K. Yamada, *Theory of Anomalous Hall Effect in Heavy Fermion System*, *J. Phys. Soc. Jpn.* **63**, 2627 (1994).
- [56] H. Kontani, T. Tanaka, D. S. Hirashima, K. Yamada, and J. Inoue, *Giant Orbital Hall Effect in Transition Metals: Origin of Large Spin and Anomalous Hall Effects*, *Phys. Rev. Lett.* **102**, 016601 (2009).
- [57] H. Kontani, T. Tanaka, and K. Yamada, *Intrinsic anomalous Hall effect in ferromagnetic metals studied by the multi-d-orbital tight-binding model*, *Phys. Rev. B* **75**, 184416 (2007).
- [58] T. Tanaka, H. Kontani, M. Naito, T. Naito, D. S. Hirashima, K. Yamada, and J. Inoue, *Intrinsic spin Hall effect and orbital Hall effect in 4d and 5d transition metals*, *Phys. Rev. B* **77**, 165117 (2008).
- [59] H. Kontani, *Anomalous transport phenomena in Fermi liquids with strong magnetic fluctuations*, *Rep. Prog. Phys.* **71**, 026501 (2008).
- [60] N. Nagaosa, J. Sinova, S. Onoda, A. H. MacDonald, and N. P. Ong, *Anomalous Hall effect*, *Rev. Mod. Phys.* **82**, 1539 (2010).

[Supplementary Materials]

Charge-loop current order and Z_3 -nematicity mediated by bond-order fluctuations in kagome metal AV_3Sb_5 (A=Cs,Rb,K)

Rina Tazai, Youichi Yamakawa, and Hiroshi Kontani

Department of Physics, Nagoya University, Nagoya 464-8602, Japan

A: Square-lattice kagome model

In Ref. [13], the present authors found that the paramagnon-interference theory naturally explains the bond-order (BO) on the basis of the kagome-lattice Hubbard model. The used lattice structure with square unit cell and its Fermi surface (FS) are shown in Figs. S1 (a) and (b), respectively. The van-Hove singular point at $\mathbf{k} = \mathbf{k}_X$ (X=A,B,C) is composed of the X-sublattice orbitals. The form factor of the 3Q BO and that of the 3Q cLC are shown in Figs. S1 (c) and (d), respectively.

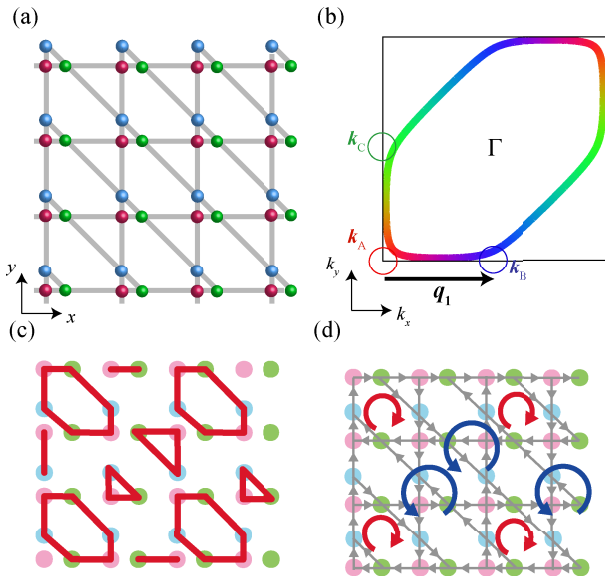


FIG. S1: (a) Square-lattice kagome metal model that is convenient for the numerical study. (b) Obtained FS in the square Brillouin zone. (c) Form factor of the 3Q BO in real space. The red bonds represent the Tri-Hexagonal pattern. (d) Form factor of the 3Q cLC. The coexistence of (c) and (d) leads to the C_6 symmetry state.

B: BO fluctuations due to Fock term by V

Here, we discuss the important effect of the nearest-neighbor Coulomb interaction V .

B-1: Hartree-Fock approximation for the U - V Hubbard model

The analysis of the kagome-lattice U - V Hubbard model based on the mean-field theory is presented in Section SF of Ref. [13]. The charge (spin) channel eigenvalue $\lambda^{c(s)}$ in the mean-field theory is given by solving the linearized DW equation with the Hartree-Fock kernel function made of U and V . Its diagrammatic expression for V is shown in Fig. S2 (a).

Figure S2 (b) shows the obtained several largest eigenvalues, λ_{SDW}^s and λ_X^c (X=CDW, BO, cLC), as functions of V/U at $U = 0.79$ [13]. These eigenvalues linearly increase with respect to U and V at a fixed V/U . When $V/U \ll 1$, a simple SDW order ($f = 1$) at $\mathbf{q} \approx \mathbf{0}$ is realized for $U \sim 1.6$. It originates from the Hartree term of U . When $V/U \gg 1$, on the other hand, simple charge-density-wave (CDW) order ($f = 1$) at $\mathbf{q} \approx \mathbf{q}_n$ is realized. In this model, $\mathbf{q}_1 = (\pi, 0)$, $\mathbf{q}_2 = (\pi, \pi)$, $\mathbf{q}_3 = (0, \pi)$. It is caused by the Hartree term of V . For $V/U = 0.4 \sim 0.65$, the BO is realized by the Fock term of V . Note that the non-local BO is not suppressed by U , while the simple CDW order due to the Hartree term of V is strongly suppressed by U . However, the cLC instability is smaller than other instabilities within the Hartree-Fock approximation.

The form factors of the BO between the nearest sites in the square kagome-lattice model in Fig. S1 (a) are given by

$$b_{AB}(\mathbf{q}) = (1 - e^{-iq_y})/2, \quad (S1)$$

$$b_{BC}(\mathbf{q}) = (1 - e^{-iq_x + iq_y})/2, \quad (S2)$$

$$b_{CA}(\mathbf{q}) = (1 - e^{iq_x})/2, \quad (S3)$$

which are normalized as $\max_{\mathbf{q}}\{b_{lm}(\mathbf{q})\} = 1$. Here, $b_{lm}(\mathbf{q}) = b_{ml}(\mathbf{q})^*$ and $b_{ll}(\mathbf{q}) = 0$.

B-2: Effective interaction due to BO susceptibility

In Fig. S2 (b), we found the development of the BO instability within the mean-field approximation. Next, we derive the effective interaction mediated by the BO susceptibility. The final result is given in Eq. (S15), which is essentially equivalent to Eq. (7) derived in the main text.

From now on, we derive Eq. (S15). First, we consider the effective interaction due to the Fock term of V . The Hamiltonian is $H_V = \sum_{il,jm} V_{il,jm} c_{il}^\dagger c_{il} c_{jm}^\dagger c_{jm}$, where i, j represent the unit cell, $l, m = A, B, C$, and c_{il} is the electron annihilation operator. (Here, we drop the spin indices for simplicity.) H_V is rewritten as $H_V = \frac{1}{N} \sum_{\mathbf{k}\mathbf{k}'\mathbf{q}\sigma\sigma'} V_{lm}(\mathbf{q}) c_{\mathbf{k}+\mathbf{q},l,\sigma}^\dagger c_{\mathbf{k},l,\sigma} c_{\mathbf{k}',m,\sigma'}^\dagger c_{\mathbf{k}'+\mathbf{q},m,\sigma'}$. Here, $V_{lm}(\mathbf{q}) = \frac{1}{N} \sum_{i,j} V_{il,jm} e^{-i\mathbf{q}\cdot(\mathbf{r}_{i,l}-\mathbf{r}_{j,m})}$, where $\mathbf{r}_{i,l}$ is the coordinate of site (i, l) : In Fig. S1 (a), $\mathbf{r}_{i,l} = (i_x, i_y)$ is independent of l , and i_x, i_y are integer coordinates. In the case of the nearest-site Coulomb interaction V , $V_{lm}(\mathbf{q})$ is expressed as

$$V_{lm}(\mathbf{q}) = 2V a_{lm}(\mathbf{q}). \quad (\text{S4})$$

Here,

$$a_{AB}(\mathbf{q}) = (1 + e^{-iq_y})/2, \quad (\text{S5})$$

$$a_{BC}(\mathbf{q}) = (1 + e^{-iq_x + iq_y})/2, \quad (\text{S6})$$

$$a_{CA}(\mathbf{q}) = (1 + e^{iq_x})/2, \quad (\text{S7})$$

where $a_{lm}(\mathbf{q}) = a_{ml}(\mathbf{q})^*$ and $a_{ll}(\mathbf{q}) = 0$. Considering the relation $a_{lm}(\mathbf{k} - \mathbf{k}') = a_{lm}(\mathbf{k})a_{lm}(\mathbf{k}')^* + b_{lm}(\mathbf{k})b_{lm}(\mathbf{k}')^*$, the Fock term $V_{lm}(\mathbf{k} - \mathbf{k}')$ in Fig. S2 (c) is expressed as

$$V_{lm}(\mathbf{k} - \mathbf{k}') = 2V[a_{lm}(\mathbf{k})a_{lm}(\mathbf{k}')^* + b_{lm}(\mathbf{k})b_{lm}(\mathbf{k}')^*]. \quad (\text{S8})$$

When $(l, m) = (A, B)$ and $(\mathbf{k}, \mathbf{k}') \approx (\mathbf{k}_A, \mathbf{k}_B)$, we obtain $a_{AB}(\mathbf{k}) \approx a_{AB}(\mathbf{k}') \approx 0$ and $b_{AB}(\mathbf{k}) \approx b_{AB}(\mathbf{k}') \approx 1$. Thus, in the Fock approximation, the form factor $g_{\mathbf{q}}^{lm}(\mathbf{k})$ derived from the DW equation is equal to $b_{lm}(\mathbf{k})$. By considering these relations, we drop a_{lm} in Eq. (S8) in the following discussion. Then, the second-order term with respect to V shown in Fig. S2 (c) is

$$(2V)^2 b_{lm}(\mathbf{k}) b_{l'm'}(\mathbf{k}')^* \chi_{lm,l'm'}^{0b}(\mathbf{q}), \quad (\text{S9})$$

where $\chi_{lm,l'm'}^{0b}(\mathbf{q}) = -\frac{T}{N} \sum_{\mathbf{p}} b_{lm}(\mathbf{p})^* G_{l'm'}(p + \mathbf{q}) G_{m'm}(p) b_{l'm'}(\mathbf{p})$.

Next, we consider all the ladder diagrams composed of the Fock terms shown in Fig. S2 (c). It is given as

$$W_{lm,l'm'}(k, k', q) \approx 2V b_{lm}(\mathbf{k}) b_{l'm'}(\mathbf{k}')^* (\hat{1} + 2V \hat{\chi}^b(\mathbf{q}))_{lm,l'm'}, \quad (\text{S10})$$

where $\mathbf{k} \approx \mathbf{k}_m$, $\mathbf{k} + \mathbf{q} \approx \mathbf{k}_l$, $\mathbf{k}' \approx \mathbf{k}_{m'}$, and $\mathbf{k}' + \mathbf{q} \approx \mathbf{k}_{l'}$. Here,

$$\hat{\chi}^b(\mathbf{q}) = \hat{\chi}^{0b}(\mathbf{q}) (\hat{1} - 2V \hat{\chi}^{0b}(\mathbf{q}))^{-1} \quad (\text{S11})$$

is the BO susceptibility. It is enlarged at $\mathbf{q} \approx \mathbf{q}_1$ only when $(lm, l'm') = (AB, AB), (AB, BA)$. (In the same way, it is enlarged at $\mathbf{q} \approx \mathbf{q}_2$ only when $(lm, l'm') = (BC, BC), (BC, CB)$.) For this reason, we can safely approximate Eqs. (S10) and (S11) as the 2×2 matrix expressions for $\mathbf{q} \approx \mathbf{q}_n$ ($n = 1, 2, 3$).

By using Eq. (S10), the charge-channel MT term in the DW equation is

$$I_{ll'mm'}(k, k', q) = 2W_{m'l'ml}(k, k+q, k'-k), \quad (\text{S12})$$

where the factor 2 comes from the summation of the parallel-spin (\uparrow, \uparrow) and the antiparallel-spin (\uparrow, \downarrow) ladder diagrams, because the Pauli principle does not work on V .

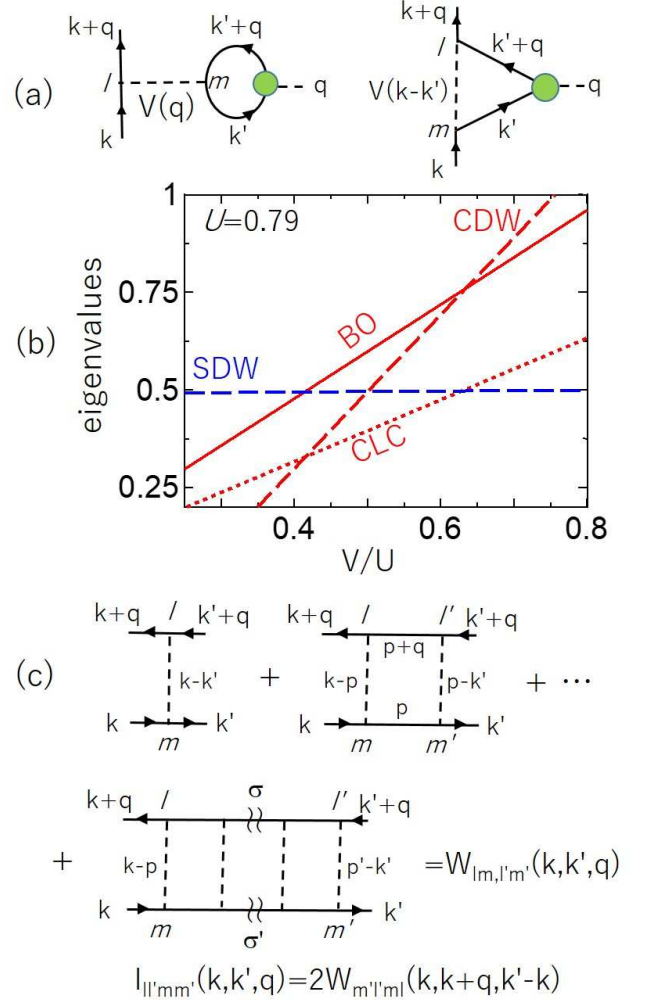


FIG. S2: (a) Hartree and Fock terms due to the on-site U and the nearest-site Coulomb interaction V in the DW equation. Green circle represents the form factor. (b) Eigenvalues of the Hartree-Fock DW equation as a function of V/U : $\lambda_{\text{SDW}}^{\text{S}}$ and $\lambda_{\text{X}}^{\text{S}}$ ($\text{X}=\text{CDW}, \text{BO}, \text{CLC}$). Note that $\lambda_{\text{BO}}^{\text{S}} \approx \lambda_{\text{BO}}^{\text{S}}$; see Ref. [13]. (c) The first- and the second-order terms with respect to the Fock terms of V . (d) Ladder-type diagrams due to the Fock terms of V . This diagram represents the BO susceptibility.

Next, we explain that the relation $\chi_{AB,AB}^b(\mathbf{q}_1) \approx \chi_{AB,BA}^b(\mathbf{q}_1)$ holds. In kagome metals, the ratio in the irreducible susceptibility $\chi_{AB,BA}^{0b}(\mathbf{q}_1)/\chi_{AB,AB}^{0b}(\mathbf{q}_1)$ is just ~ 0.2 because the Green function $G_{lm}(\mathbf{k})$ is nearly diagonal ($\propto \delta_{l,m}$). Nonetheless of this fact, the ratio

in the BO susceptibility $R \equiv \chi_{AB,BA}^b(\mathbf{q}_1)/\chi_{AB,AB}^b(\mathbf{q}_1)$ is of order unity, when the BO Stoner factor $\alpha_{BO} = 2V(\chi_{AB,AB}^{0b}(\mathbf{q}_1) + \chi_{AB,BA}^{0b}(\mathbf{q}_1))$ is close to unity. In fact, for $\mathbf{q} \approx \mathbf{q}_1$, the relation between the BO susceptibility and its irreducible susceptibility is $\hat{\chi}^b = \hat{\chi}^{b0} + 2V\hat{\chi}^{b0}\hat{\chi}^b$, where $\hat{\chi}^{b0}$ is the 2×2 matrix: $\hat{\chi}^{b0} = \begin{pmatrix} \chi_{AB,AB}^{b0} & \chi_{AB,BA}^{b0} \\ \chi_{BA,AB}^{b0} & \chi_{BA,BA}^{b0} \end{pmatrix}$. Then, the BO susceptibility for $\mathbf{q} \approx \mathbf{q}_1$ is obtained as

$$\chi_{AB,AB}^b(q) = [a - 2V(a^2 - b^2)]/d, \quad (\text{S13})$$

$$\chi_{AB,BA}^b(q) = b/d, \quad (\text{S14})$$

where $a \equiv \chi_{AB,AB}^{0b}(q)$, $b \equiv \chi_{AB,BA}^{0b}(q)$, and $d \equiv (1 - (a + b)2V)/(1 - (a - b)2V)$.

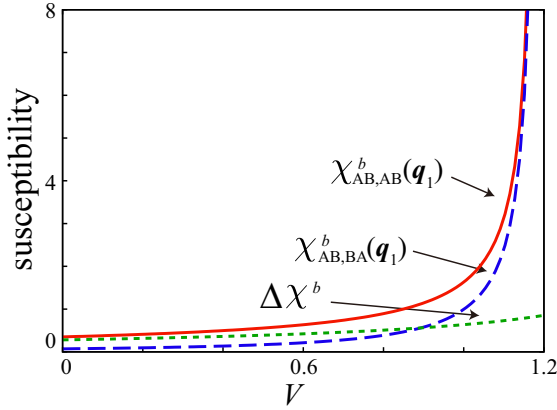


FIG. S3: $\chi_{AB,AB}^b$ and $\chi_{AB,BA}^b$ given in Eqs. (S13) and (S14) as function of V . We set $a = 0.35$ and $b/a = 0.2$. $\Delta\chi^b \equiv \chi_{AB,AB}^b - \chi_{AB,BA}^b$ is also shown.

According to Eqs. (S13) and (S14), R becomes $b/a (\ll 1)$ when $V = 0$. In contrast, we obtain $R \approx 1$ at $\alpha_{BO} \approx 1$ ($\alpha_{BO} = (a + b)2V$). Figure S3 shows the BO susceptibilities $\chi_{AB,AB}^b$ and $\chi_{AB,BA}^b$ as functions of V . We set $a = \chi_{AB,AB}^{b0}(\mathbf{q}_1) = 0.35$ and $b/a = 0.2$. Both $\chi_{AB,AB}^b$ and $\chi_{AB,BA}^b$ increase with V , while $\Delta\chi^b \equiv \chi_{AB,AB}^b - \chi_{AB,BA}^b$ is almost constant. This result means that the relation $R \approx 1$ holds near the BO-endpoint, around which the relation $\alpha_{BO} \lesssim 1$ holds.

According to Eqs. (S10) and (S12), in the case of $R \approx 1$, the MT kernel function for the DW equation is simply given as

$$I_{l',mm'}(k, k', q) \approx g_{k'-k}^{m'l'}(k) g_{k-k'}^{lm}(k' + q) \times 2(2V)^2 \chi^b(k - k'), \quad (\text{S15})$$

where $\chi^b(q) \equiv \chi_{AB,AB}^b(q) + \chi_{AB,BA}^b(q) \approx \chi_{AB,AB}^{b0}(q)/(1 - \alpha_{BO}(q))$ for $\mathbf{q} \approx \mathbf{q}_1$, and $g^{lm} \approx b_{lm}$ is the normalized BO form factor derived from the DW equation [13]. Equation (S15) is equal to Eq. (7) in the main text with $y = 2$. Note that both charge- and three spin-channel BO fluctuations develop in the present off-site V mechanism.

To summarize, the relation $\chi_{AB,AB}^b \approx \chi_{AB,BA}^b$ (*i.e.*, $R \approx 1$), which is assumed in the cLC mechanism in the main text, is well satisfied in the off-site V mechanism. Because this relation is also satisfied in the paramagnon-interference mechanism [13] and the phonon mechanism, these three different BO mechanisms will cooperate. We consider that the main mechanism of the BO in kagome metals is the paramagnon interference mechanism [13], and both the bond-stretching phonon mode and the off-site Coulomb interaction will assist the BO formation.

C: Effects of AL-type VCs

Here, we examine the role of the Aslamazov-Larkin (AL) vertex corrections (VCs) due to the interference between two bosonic susceptibilities (χ^{boson}) shown in Fig. S4. The AL terms are significant for the even-parity order parameter in the paramagnon-interference mechanism. This mechanism is responsible for the BO and the orbital order in Fe-based superconductors [27, 31, 32], high- T_c cuprates [29, 30, 51, 51], and kagome metals [13]. In contrast, the AL term is unimportant for the odd-parity order parameter, and instead, the Maki-Thompson (MT) term is significant for the current order in the frustrated Hubbard models [50] and non-Fermi liquid transport phenomena [59].

Here, we explain that the AL terms due to the bond-susceptibilities, which were neglected in the main text, are unimportant in the present cLC mechanism in kagome metals. Figure S4 exhibits the VC for $f_{\mathbf{q}_1}^{\text{AB}}(\mathbf{k})$ at $\mathbf{k} \approx \mathbf{k}_A$. These terms are almost canceled for the odd-parity cLC order because of the relation $f_{\mathbf{q}_1}^{\text{AB}}(\mathbf{k}) = -f_{\mathbf{q}_1}^{\text{BA}}(-\mathbf{k} - \mathbf{q})$. In fact, the order parameter in the real space satisfies the relation $\delta t_{ij} = \mathcal{P}\delta t_{ji}$, where $\mathcal{P} = +1$ (-1) for the even (odd) parity order and $l, m = A, B, C$. Then, its Fourier transform gives the form factor:

$$\begin{aligned} f_{\mathbf{q}}^{lm}(\mathbf{k}) &= \frac{1}{N} \sum_i^{\text{sub-l}} \sum_j^{\text{sub-m}} \delta t_{ij} e^{-\mathbf{k} \cdot (\mathbf{r}_i - \mathbf{r}_j)} e^{-\mathbf{q} \cdot \mathbf{r}_j} \\ &= \frac{1}{N} \sum_i^{\text{sub-l}} \sum_j^{\text{sub-m}} (\mathcal{P}\delta t_{ji}) e^{-\mathbf{k} \cdot (\mathbf{r}_i - \mathbf{r}_j)} e^{-\mathbf{q} \cdot \mathbf{r}_j} \\ &= \mathcal{P} f_{\mathbf{q}}^{ml}(-\mathbf{k} - \mathbf{q}). \end{aligned} \quad (\text{S16})$$

In addition, it is verified that each AL term in Fig. S4 is small because the momentum summation is restricted by four g 's. (Note that $|g_{\mathbf{q}}^{lm}(\mathbf{k})| \leq 1$.)

D: Stability of the nematic BO+cLC state

In the main text, we explained that the coexistence of the $3Q$ BO and the $3Q$ cLC leads to one C_6 state and

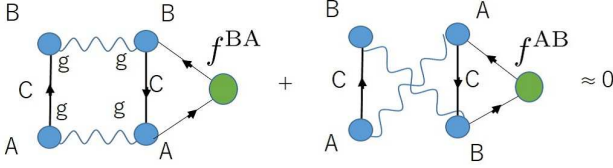


FIG. S4: Two AL terms for the cLC order at $\mathbf{q} = \mathbf{q}_1$. These terms are almost canceled for the cLC order with $f_{\mathbf{q}_1}^{\text{AB}}(\mathbf{k}) = -f_{\mathbf{q}_1}^{\text{BA}}(-\mathbf{k} - \mathbf{q}_1)$.

three nematic (C_2) states. Here, we discuss the stability of these four states based on the Ginzburg-Landau (GL) theory. It is found that the nematic states are expected to emerge when $T_{\text{BO}} > T_{\text{cLC}}$ by considering the third-order GL terms, which play essential roles in kagome metals.

Here, we define the BO form factors and the cLC form factors by Figs. S1 (c) and (d), respectively. Then, the BO form factors $g_{\mathbf{q}_1}^{\text{AB}}(\mathbf{k})$, $g_{\mathbf{q}_2}^{\text{BC}}$ and $g_{\mathbf{q}_3}^{\text{CA}}$ are given by Eqs. (S1)-(S3), respectively. The relation $g_{\mathbf{q}}^{lm}(\mathbf{k}) = \{g_{\mathbf{q}}^{ml}(\mathbf{k})\}^*$ is satisfied. The BO parameter is $\phi_{lm}(g_{\mathbf{q}}^{lm} + g_{\mathbf{q}}^{ml})$ ($lm = \text{AB}, \text{BC}, \text{CA}$). Here, we introduce the vector representation $\phi \equiv (\phi_{\text{AB}}, \phi_{\text{BC}}, \phi_{\text{CA}})$, and define $\phi_0 \equiv (\phi, \phi, \phi)/\sqrt{3}$, $\phi_1 \equiv (-\phi, \phi, \phi)/\sqrt{3}$, $\phi_2 \equiv (\phi, -\phi, \phi)/\sqrt{3}$, and $\phi_3 \equiv (\phi, \phi, -\phi)/\sqrt{3}$. When $\phi = \phi_0$, we obtain the Tri-Hexagonal (Star-of-David) pattern for $\phi > 0$ ($\phi < 0$) shown in Fig. S1 (c). Note that the free energy for ϕ is different from that for $-\phi$ due to the third order term. When $\phi = \phi_i$ ($i = 1 \sim 3$), we obtain the Tri-Hexagonal pattern for $\phi < 0$, while it is displaced by \mathbf{a}_{lm} from Fig. S1 (c).

Also, we assume that the cLC form factors are approximately given as $f_{\mathbf{q}}^{lm}(\mathbf{k}) = -ig_{\mathbf{q}}^{lm}(\mathbf{k})$ for $lm = \text{AB}, \text{BC}, \text{CA}$, and $f_{\mathbf{q}}^{lm}(\mathbf{k}) = ig_{\mathbf{q}}^{lm}(\mathbf{k})$ for $lm = \text{BA}, \text{CB}, \text{AC}$. The cLC order parameter is $\eta_{lm}(f_{\mathbf{q}}^{lm} + f_{\mathbf{q}}^{ml})$. We introduce the notation $\eta \equiv (\eta_{\text{AB}}, \eta_{\text{BC}}, \eta_{\text{CA}})$, and define $\eta_0 \equiv (\eta, \eta, \eta)/\sqrt{3}$, $\eta_1 \equiv (-\eta, \eta, \eta)/\sqrt{3}$, $\eta_2 \equiv (\eta, -\eta, \eta)/\sqrt{3}$, and $\eta_3 \equiv (\eta, \eta, -\eta)/\sqrt{3}$. The cLC pattern in Fig. S1 (d) is given by $\eta = \eta_0$ with $\eta > 0$, and the direction of the cLC is reversed when $\eta < 0$. Note that the free energy for η is equal to that for $-\eta$. When $\eta = \eta_i$ ($i = 1 \sim 3$), the cLC pattern is given by the parallel shift of Fig. S1 (d) by \mathbf{a}_{lm} .

Now, we set $\phi = \phi_0$. When $\eta = \eta_0$, the BO+cLC state is C_6 -symmetric, because the superposition of Figs. S1 (c) and (d) becomes Fig. 5 (a) in the main text. When $\eta = \eta_i$ ($i = 1 \sim 3$), the BO+cLC state is C_2 -symmetric shown in Fig. 5 (c) in the main text.

Hereafter, we construct the GL free energy up to the fourth-order terms:

$$F = F^{(2)} + F^{(3)} + F^{(4)}, \quad (\text{S17})$$

The second-order term is

$$F^{(2)} = a_1|\phi|^2 + a_2|\eta|^2, \quad (\text{S18})$$

$$a_1 = -\chi_g^0(\mathbf{q}_1) + I_b^{-1}, \quad (\text{S19})$$

$$a_2 = -\chi_f^0(\mathbf{q}_1) + I_c^{-1}, \quad (\text{S20})$$

where $I_{b(c)}$ (> 0) is the effective interaction for the BO (cLC order) [12, 51]. ($a_{1,2} \leq 0$ corresponds to $\lambda_{\mathbf{q}} \geq 1$ in the DW equation as proved in Ref. [51].) Because $\chi_g^0(\mathbf{q}_1) \approx \chi_f^0(\mathbf{q}_1)$, the relation $T_{\text{BO}} > T_{\text{cLC}}$ would be realized when $I_b > I_c$. We note that, in the present theory, both I_b and I_c originate from the electron correlations, and therefore they exhibit strong T -dependences.

The third order term and the fourth order term for general ϕ and η are given as

$$\begin{aligned} F^{(3)} &= b_1\phi_1\phi_2\phi_3 + b_2(\phi_1\eta_2\eta_3 + \eta_1\phi_2\eta_3 + \eta_1\eta_2\phi_3), \quad (\text{S21}) \\ F^{(4)} &= d_{1,a}(\phi_1^4 + \phi_2^4 + \phi_3^4) + d_{1,b}(\phi_1^2\phi_2^2 + \phi_2^2\phi_3^2 + \phi_3^2\phi_1^2) \\ &\quad + d_{2,a}(\eta_1^4 + \eta_2^4 + \eta_3^4) + d_{2,b}(\eta_1^2\eta_2^2 + \eta_2^2\eta_3^2 + \eta_3^2\eta_1^2) \\ &\quad + 2d_{3,a}(\phi_1^2\eta_1^2 + \phi_2^2\eta_2^2 + \phi_3^2\eta_3^2) \\ &\quad + d_{3,b}(\phi_1^2\eta_2^2 + \phi_2^2\eta_3^2 + \phi_3^2\eta_1^2 + \phi_2^2\eta_1^2 + \phi_3^2\eta_2^2 + \phi_1^2\eta_3^2), \quad (\text{S22}) \end{aligned}$$

where we denote $(\phi_{\text{AB}}, \phi_{\text{BC}}, \phi_{\text{CA}}) \equiv (\phi_1, \phi_2, \phi_3)$ and $(\eta_{\text{AB}}, \eta_{\text{BC}}, \eta_{\text{CA}}) \equiv (\eta_1, \eta_2, \eta_3)$. (The term $\sim \phi_1\phi_2\eta_1\eta_2$ is absent.) In the absence of the cLC order, the third-order free energy term is given by the first term of Eq. (S21). The diagrammatic expression for the coefficient b_1 is given in Fig. S5 (a), and its analytic expression is found in Refs. [12, 53]. When the BO and the cLC coexist, we obtain the additional cross-terms given by the second term of Eq. (S21). The diagrammatic expression for b_2 is given in Fig. S5 (b). The relation $b_1 = -b_2$ holds when the relation $f_{\mathbf{q}_2}^{\text{BC}}(\mathbf{k}_C)f_{\mathbf{q}_3}^{\text{CA}}(\mathbf{k}_A) = -g_{\mathbf{q}_2}^{\text{BC}}(\mathbf{k}_C)g_{\mathbf{q}_3}^{\text{CA}}(\mathbf{k}_A)$ holds. Note that the minimum of the GL free energy does not diverge due to the positive fourth-order term.

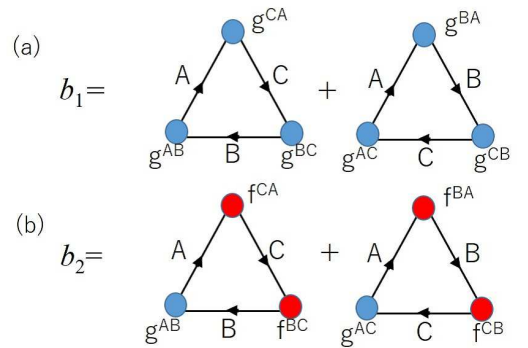


FIG. S5: Diagrams for the third-order terms b_1 and b_2 . The relation $b_1 = -b_2$ holds when $f_{\mathbf{q}}^{lm}(\mathbf{k}) = \pm ig_{\mathbf{q}}^{lm}(\mathbf{k})$.

Here, we discuss the possible $3Q$ BO+cLC states in the case of $T_{\text{BO}} > T_{\text{cLC}}$. We recall that the BO+cLC state with $\phi = \phi_0$ and $\eta = \eta_0$ ($= \eta_i; i = 1 \sim 3$) has C_6 (C_2) symmetry in the present notation. Then, the third

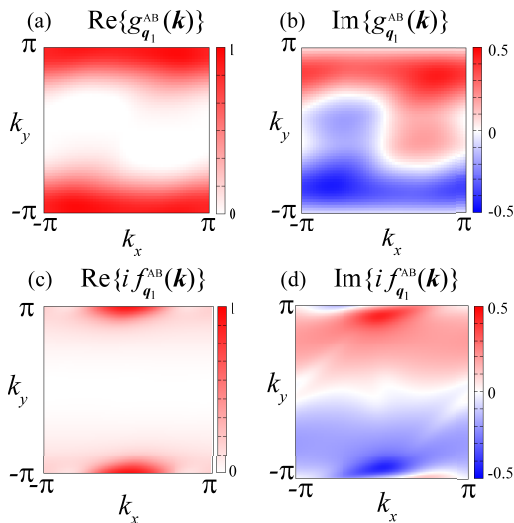


FIG. S6: Obtained (a) real part and (b) imaginary part of the BO form factor $g_{q_1}^{AB}(\mathbf{k})$ in the square kagome-lattice model. The approximate relation $g_{q_1}^{AB}(\mathbf{k}) \approx \frac{1}{2}(1 - e^{-ik_y})$ means that the BO is mainly formed between the nearest sites. Obtained (c) real part and (d) imaginary part of the cLC form factor $if_{q_1}^{AB}(\mathbf{k})$. Its strong \mathbf{k} -dependence means the existence of large cLC order between distant sites.

order term is

$$F^{(3)'} = (b_1/3\sqrt{3})\phi(\phi^2 + s|b_2/b_1|\eta^2), \quad (\text{S23})$$

where $s = -3$ for $\boldsymbol{\eta} = \boldsymbol{\eta}_0$, and $s = +1$ for $\boldsymbol{\eta} = \boldsymbol{\eta}_i$, because of $b_1 b_2 < 0$. Just below T_{BO} , the Star-of-David BO $\phi < 0$ (Tri-Hexagonal BO $\phi > 0$) is realized for $b_1 > 0$ (< 0). Just below T_{cLC} , to get the energy-gain from $F^{(3)}$ in Eq. (S21), the parameter $s = +1$ is selected irrespective of the sign of b_1 . (The $(3Q \text{ BO})+(1Q \text{ cLC})$ state is also unfavorable for $|\eta| \ll |\phi|$.) Thus, we obtain the nematic BO+cLC state shown in Fig. 5 (c) in the main text.

Thus, the Z_3 nematic BO+cLC state shown in Fig. 5 (c) in the main text is expected to be realized for $T < T_{\text{cLC}} < T_{\text{BO}}$, irrespective of the sign of b_1 in Eq. (S21). More specifically, the C_2 BO+cLC state is realized when

$|b_1/b_2|(\phi/\eta)^2 > 1$, while the C_6 BO+cLC state ($s = -3$) is realized in the opposite case.

Finally, we discuss the fourth-order GL term in Eq. (S22). The coefficients $d_{l,a}$ and $d_{l,b}$ ($l = 1, 2, 3$) are positive, and they are given by the closed Feynman diagrams made of four form factors and four G 's [12]. The relations $d_{1,a} = d_{2,a} = d_{3,a}$ and $d_{1,b} = d_{2,b} = d_{3,b}$ hold in the case of $f_{\mathbf{q}}^{lm}(\mathbf{k}) \approx \pm i g_{\mathbf{q}}^{lm}(\mathbf{k})$. For any $\phi = \phi_\alpha$ and $\boldsymbol{\eta} = \boldsymbol{\eta}_\beta$ ($\alpha, \beta = 0 \sim 3$), the fourth-order GL term is expressed as

$$F^{(4)'} = d_1 \phi^4 + d_2 \eta^4 + 2d_3 \phi^2 \eta^2, \quad (\text{S24})$$

where the coefficients are $d_1 = (d_{1,a} + d_{1,b})/3$, $d_2 = (d_{2,a} + d_{2,b})/3$, and $d_3 = (d_{3,a} + d_{3,b})/3$. These fourth-order GL terms can cause interesting $1Q$ - $3Q$ phase transitions at low temperatures.

We stress that the relation $f_{\mathbf{q}}^{lm}(\mathbf{k}) \approx \pm i g_{\mathbf{q}}^{lm}(\mathbf{k})$ is not satisfied as shown in Figs. S6 (a)-(d), because the mechanisms of the cLC and the BO are different in the present theory. Therefore, all the coefficients b_l , $d_{m,a}$, $d_{m,b}$ depend on $l = 1, 2$ and $m = 1, 2, 3$. We recently calculated b_1 and b_2 by using the form factors in Fig. S6, and obtained the relation $-b_2/b_1 \approx 2$. The relation $-b_2/b_1 \gg 1$ is favorable for the $3Q$ BO+cLC coexisting phase, as understood from Eq. (S23). It is an important future issue to calculate all the GL coefficients b_l , $d_{m,a}$, $d_{m,b}$ microscopically. The present GL analysis indicates that various interesting BO+cLC coexisting phases are realized in kagome metals.

Before closing this section, we consider the case of $T_{\text{cLC}} > T_{\text{BO}}$. Just below T_{cLC} , the third-order term given by Eq. (S21) is absent. Then, the $1Q$ cLC $\boldsymbol{\eta} = (\eta, 0, 0)$ appears for $d_{2,b}/2d_{2,a} > 1$ according to Eq. (S22). (The $3Q$ cLC $\boldsymbol{\eta}_\alpha$ ($\alpha = 0 \sim 3$) appears for the opposite case.) We recently obtained the relation $d_{2,b}/2d_{2,a} \approx 1$ by using the cLC form factor in Figs. S6 (c) and (d). When $d_{2,b}/2d_{2,a} > 1$, the $(3Q \text{ BO})+(1Q \text{ cLC})$ state is realized just below T_{BO} . However, it may change to the C_6 symmetry $(3Q \text{ BO})+(3Q \text{ cLC})$ state at lower T due to the third order GL term for $|b_1/b_2|(\phi/\eta)^2 < 1$, as we discussed above.